Manchester Metropolitan University

e-space

Manchester Metropolitan University's Research Repository

Please cite the Published Version

Behera, Ajit, Saxena, Kuldeep, Prakash, Chander, Pramanik, Alokesh, Haider, Julfikar, Basak, Animesh and Shankar, S (2023) Modeling and Simulation of Magnetron Sputterred NiTi Thin Film Deposition by SRIM/TRIM. Surface Review and Letters. ISSN 0218-625X

DOI: https://doi.org/10.1142/s0218625x2340005x

Publisher: World Scientific Publishing

Version: Accepted Version

Downloaded from: https://e-space.mmu.ac.uk/631214/

Usage rights: © In Copyright

Additional Information: Electronic version of an article published as Surface Review and Letters, 2023, Online Ready, https://doi.org/10.1142/S0218625X2340005X © copyright World Scientific Publishing Company https://www.worldscientific.com/doi/10.1142/S0218625X2340005X

Enquiries:
If you have questions about this document, contact openresearch@mmu.ac.uk. Please include the URL of the record in e-space. If you believe that your, or a third party's rights have been compromised through this document please see our Take Down policy (available from https://www.mmu.ac.uk/library/using-the-library/policies-and-guidelines)

Magnetron sputtering deposited NiTi thin film modeling using Stopping and Range of Ions in Matter

Ajit Behera[1], Kuldeep Saxena[2], Chander Prakash[3], Alokesh Pramanik[4], Julfikar Haider[5], Sandeep Kumar[6], Gaurav Kumar[7*]

[1]Department of Metallurgical & Materials Engineering, National Institute of Technology, Rourkela, Odisha-769008, ajit.behera88@gmail.com

[2]Department of Mechanical Engineering, GLA University, Mathura-281406, India, saxena0081@gmail.com

[3]School of Mechanical Engineering, Shandong University of Technology, Zibo, China

[4]Department of Mechanical Engineering, Curtin University, Australia

[5]Department of Engineering, Manchester Metropolitan University, UK

[6]Division of Research & Innovation, Uttaranchal University, Uttarakhand, 248007, Dehradun, India

[7]Department of Mechanical Engineering, Chandigarh University, Mohali, India

---

[*]**Corresponding author**: Dr. Gaurav Kumar, gauravcivilengg714@gmail.com

Abstract

Nickel-Titanium thin films have gained a lot of attention as functional materials in recent years due to its unique features such as the shape memory effect. Micro-actuators, micro-valve, micro-fluid pumps, bio-medical applications, and electronic applications has a lot of interest because of these smart thin films. It has ability to recover substantial transformation stress and strain when heated and cooled. SMAs thin films have a number of additional characteristics, including pseudoelasticity, good corrosion resistance, great damping capacity, good biocompatibility. Sputter-deposited NiTi thin films have been discovered to be very useful as powerful actuators in micro-electro-mechanical systems (MEMS) because of its large recovery forces and high recoverable strains. Despite the advancement of improved deposition method for NiTi thin films, there are still certain unsolved difficulties that impede accurate composition control throughout deposition process. Many applications, spanning from aerospace industries to a range of nanotechnologies, require knowledge of sputtering properties of materials which is due to ejection, bombardment and deposition of ions. In recent decades, atomic scale modelling has been given a high emphasis in ion sputtering research, providing a pretty precise description of collisions cascades in solids using the SRIM/TRIM. In this paper, SRIM which is usually used to figure out how heavy ions interact with the target materials. A variety of ion-solid interaction properties, including the sputter yield, is determined by simulating collision cascades in solids. TRIM is used to describe the range of ions that enter the matter, also the damage aspects done to target throughout the process. The simulation is done to compare sputtering yield of nickel and titanium by varying the energy input. SRIM simulation is conducted by varying the thickness of the film, angle of incidence of ions and energy involved in the sputtering process. Characterization of the film has been carried out using FESEM to know the surface and interface morphology for the validation of simulated results.

Keywords: Thin film, Magnetron Sputtering, NiTi, ions, Deposition, Energy, Angle of incident

1. Introduction

SMA is the most important kind of advanced material among various type of shape memory materials [1-2]. SMAs possesses unique intrinsic properties that can be used in a smart device. In SMAs, there are commonly two primary crystallographic structures i.e. low-temperature martensite phase and high-temperature austenite phase. The shape recovery behavior of shape memory materials are usually caused by a crystallographic structural change. SMAs are easily deformed at the low-temperature martensite phase, but when energy is applied, they change to the austenitic phase (parent phase) and regain their original shape [3]. SMA responds very quickly to external stimuli/inputs like electric field, magnetic field, heat, stress etc. For actuators, SMAs can produce huge displacements and enormous forces. The features of phase change and reverse back to original phase repeatability are exceptional as comparison with other smart materials. SMAs have a relatively high damping capacity [4-5]. With no design complexity, shape memory actuators can operate in any conditions like tensile, compressive, twisting, rotating, or a hybrid of such deformation behavior. The two important properties exist in NiTi thin film SMA such as shape memory effect (SME) and pseudoelasticity. SME describes the capability of materials to return to their original shape even after going through extreme deformation. This effect is based on phase transformation between austenite and martensite phases on changing temperature or application of stress. Figure 1(a) represents the stress-strain-temperature plot for SME in NiTi. Here, the high-temperature parent phase austenite is shown at point 4, and on cooling, austenite starts transforming into a low-temperature daughter phase called twinned martensite shown at point 1. The twinned martensite has low symmetry compared to the parent phase, so deformation is

possible on increasing the stress. When the applied pressure crosses σs (starting level stress), the reorientation takes place in twinned martensite, and slowly it transforms into detwinned martensite shown at point 2. This de-twinning process gets completed when stress reaches a final level of stress (σf). On unloading, the material retains to de-twinned martensite structure at point 3. The stress-free martensite is subjected to temperature rise, and phase transfer takes to austenite i.e. shown at point 1. This transformation starts when the applied temperature crosses the austenite starting temperature (As) and ends when the temperature reaches austenite finish temperature (Af). Now material goes to its former position 1 (parent phase). The process is continuous in cycles with changing temperature and stress the material comes to its former state; this phenomenon is called the SME. The second property, pseudoelasticity exhibits by SMA which describes rubber-like behavior. SMA's elastic nature is related to stress induced transformation by raising the temperature above that of the transition temperature with a constant level. As we increase the load, strain is generated when the temperature is greater than the finish temperature of austenite (Af.). Upon maintaining high temperature and unloading it, there would be strain recovery. This reversible transformation is caused due to thermomechanical loading path. Instead of transforming between phases, there will be the recovery of large strains when the temperature is above Af. Figure 1(b) represents the stress-strain curve of SMA pseudoelasticity. The cycle keeps on going, (1-2-1) curve is called as pseudoelastic curve [6-8].

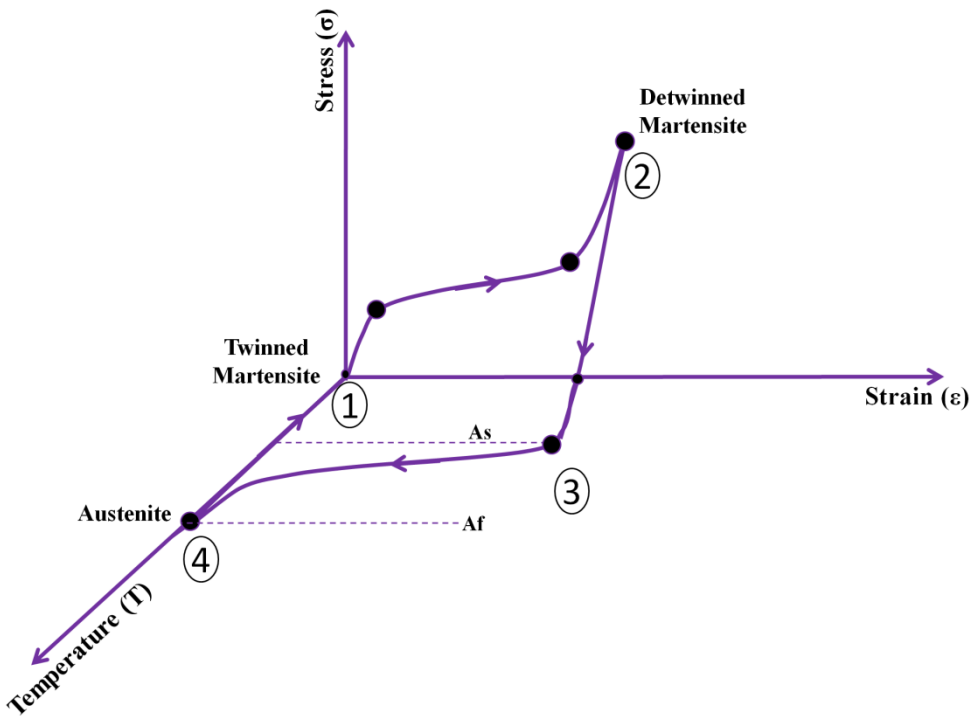

Figure 1: (a) Shape memory effect, (b) Pseudoelasticity of Ni-Ti SMA

Because of its unique properties, such as huge force/stroke, periodical action, and functioning ability in extreme conditions (space, corrosive environment, radio-active and biological), NiTi SMAs thin film is used as the primary technology for actuating number of MEMS nanotechnology devices (space, radioactive, corrosive and biological). In the recent decade, sputter-deposited SMA thin films have received a lot of interest. NiTi-based thin films could improve microscale instruments such as gyroscopes, accelerometers, sensors, microphones, micro-scanners, and optical switches used in automotive, aerospace, biomedical, electronic instrumentation, and military applications [9]. The advantages of Ni-Ti thin film are: 1) good mechanical performances, 2) less voltage for operation, 3) significant deformation with large actuation-forces, 4) the power-to-weight ratio is higher, 5) exceptional corrosion, wear and chemical resistance, 6) good frequency responses, 7) light-weight and compact. Whereas, disadvantages of NiTi thin film are, 1) low energy efficiency, 2) low operational speed and large hysteresis, 3) complex thermo-mechanical properties, 4) NiTi films are expensive, and

controlling their composition as well as mechanical performance is challenging, 5) complex motion control, 6) temperature dependent effect, 7) poor fatigue properties [10-13].

This paper deals with the fabrication of double-bi-layered NiTi thin film using DC/Rf Magnetron Sputtering technique. The novel studies has been carried out are, 1) to compare the sputtering yield of Nickel and Titanium by varying energy input, 2) to study the variation of sputtering yield with angle of incidence using SRIM and TRIM, 3) to analysis of energy input, thickness of deposition, and angle of incidence to develop the NiTi thin film, 4) to study the surface and interface morphology of the sputtered thin film using FESEM.

2. Materials and Method

Nickel-Titanium film has been grown at room temperature on silicon substrates with different elemental Ni (99.9 % purity) and Ti (99.9 % purity) targets. Prior to the use, substrate must be cleaned properly without any contaminants, as per the ref [14]. The DC/rf magnetron sputtering is used with the parameters as given in table 1 to develop the double bi-layered NiTi thin film. It is essential to pick parameters carefully in order to get the desired NiTi thin film properties. To control deposition factors, one parameter was changed, keeping the rest constant. Three sputter gun units are present in the equipment and 415 mm x 800 mm x 1868.19 mm is the overall system size. The main deposition chamber is cylindrical stainless steel chamber with 305 mm internal diameter and 125 mm depth. The enclosure is evacuated by a turbo-molecular pump (Model: Alcatel ATP series) to a base pressure of 5x10-6 mbar with Ar/N2 gas just before deposition stage. To control the pressure of the thin films, a variable mixture of Ar and N2 had to be supplied throughout the sputtering process. Initially, argon and nitrogen gas were delivered through mass flow controllers with valves in front of them to ensure that the supply may be stopped off at any time. Then the gases were sent via a tube loaded with glass balls, which assured proper mixing. The amount of gas introduced to

the chamber and hence the pressures throughout the process were controlled by an on/off and a needle valve. The gas were made to pass into the chamber via a ring-shaped stainless steel tube that encircled the cathode. The target is manufactured using a standard powder processing method. In the depositing procedure, highly-pure (99.99 percent) targets with a diameter of 6 inches and a thickness of 2.5 inches were utilized, with DC power supplied. The target was 125 mm away from the substrate plate. The targets were positioned in such a manner that it comprise the strong magnetic field that improves the ionization energy of the target. Even at low pressure, the magnetron gun can produce plasma close to the target. A substrate heater is being used to heat the substrates during and after deposition up to a maximum temperature of 850°C. The substrate is rotated to ensure uniformity in thickness and composition utilizing RPM control volume (NP100). Double bi-layer on the substrate has been developed in the sequence Ti-Ni-Ti-Ni. The field emission scanning electron microscopy (Carl Zeiss-SUPRA40) is used to examine NiTi thin film surface and interface morphologies, defects, and topologies of the specimen.

Table 1: Parameters of sputtering process.

Sputtering Parameter	Optimized value
Partial gas pressure	5 mTorr
Gas flow rate	50 sccm
Substrate to target distance	125 mm
Ni power	
Ti power	

There are two modeling tool used to analyze the sputtering deposition procedure such as ‘stopping and range of ions in matter (SRIM)’ and ‘Transport of Ions in Matter (TRIM)’ [15-16]. SRIM is usually used to figure out how heavy ions interact with the target materials

using the Monte Carlo simulation based on binary collision approximation to predict the expected range, energy involved in deposition, and other physical features of ion irradiation. The sputtering technique and interactions of species produced at Ni and Ti target with Ar gas ions entering the substrate were described using simulations. SRIM is primarily concerned with determining how ions loses energy onto the matter and their overall distributions after they have slowed inside the targets. This also relates with both the movement of lattice atom generated by high-energy collision and the formation of plasmon inside the solid. Thermal impacts within solids, especially rearrangement of lattice-atom or thermally induced implantations of ions or diffusions caused by vacancies, are not investigated. The main purpose of this research is to develop methods for calculating the stopping and range of ions using precise experimental data and then expanding these values using unified theoretical principles. TRIM is a complex software that relate not only the range of particles which can penetrate into the matter, as well as a variety of other characteristics about the harm caused to the targets during the process of slowing down of the particles, also about the thin film deposition by sputtering. This demonstrates how particles enter into the target instantaneously, along with recoiling cascade and target particles mixing. TRIM calculates the physics of each interaction between an energetic ion and a target atom for one ion at a time to produce precise evaluations of the physics of each collision. This calculation can take anywhere from a few seconds to several minutes for each ion. TRIM can be used for basic calculations like those found in the stopping and range (SR) tables, which take as little as a second to complete, or for comprehensive calculations like details of damage produced, ions interactions, which can take several hours to complete for 100 ions.

First we are using SRIM to set the Ion data and target data. Here it is taking ion data as Argon and target data as double bi-layer of Ni/Ti. To have choosen the required element by the periodic table available in the softwere package. Similarly, in the target section we set double

bi-layered of Ni/Ti. On clicking calculate table we get a table which consist of range of ion energy as well as depth (thickness). We have choosen respective ion energy for respective depth required. Using this energy value we will then operate in TRIM. Then we used TRIM to calculate the entire profile and assess the damage. The final stage is to see if the target has developed an amorphous layer. In ion data section, we can choose the type of TRIM calculation. We choose detailed calculation with full damage cascades which analysis all collisional damage to the target. Ti-Ni-Ti-Ni is chosen for the required double bi-layer thin film. Here we can only chose ions and not molecules. For parameters of ions data the atomic number and mass number is default of the implant ion. We can change the implantation energy as obtained from SRIM simulation i.e. step 1. The angle of incidence here is the ion implantation angle through which ions will strike the surface of the substrate. Coming to the second part that is the target data, the default target material of the program is set as single layer, as a aim is to produce double bi-layer Ni-Ti we can click on "Add new layer" on the right side of the section setting for target material is present. We have to set Ti-Ni-Ti-Ni by clicking periodic table button and added new layers accordingly. The parameters of the ions like density, atomic number are filled by default. At last we click on "Save Input and Run Trim". The sputtering yield is basically calculated using the SRIM-TRIM software for both nickel and titanium using Ar as the sputtering gas. The target is generally taken in elemental form and sputtering yield is generally calculated separately for Ni and Ti. As sputtering is a surface phenomenon a bulkier target is taken with thickness of 200Å. It is run under detailed calculation with full damage cascade mode in TRIM.

The targets were sputtered using different target energies. The energies were taken generally as 300 V, 500 V, 700 V, 1100 V and 1300 V [23]. In addition, the simulations is carried out at different angle of incidence i.e. at 0°, 30° and 45°. The target atoms are bombarded by

uniform argon ions at different energy level [24]. All the variation of parameters has been given in the table 2.

Table 2: Input parameters involved in the simulation.

Parameters	Input values
Total number of atoms for simulations	90000
Sputtering Energies	300 V, 500 V, 700 V, 1100 V, 1300 V
Target thickness	200 Å
Angle of incidence	0°, 30°, 45°
Sputtering gas	Argon
Target materials	Nickel (Ni) and Titanium (Ti)
Density of nickel	8.89
Density of titanium	4.52
Lattice binding energy	3 ev
Displacement energy	25 ev
Surface binding energy of nickel	4.46 ev
Surface binding energy of titanium	4.89 ev

3. Results and Discussions

3.1. Sputtering yield with the variation of input energies

By varying the energy level with keeping all other parameter constant, it is observed that the sputtering yield for both the element increases. The sputtering yield of Ni is found greater than that of Ti (Figure 2(a)) [17]. This is because sputtering efficiency of nickel is more than titanium. The sputtering yield depends on the target voltage, type of target etc. As the sputtering yield is different for both nickel and titanium it may hamper the uniformity of the film. With the variation of the voltage 300 V, 500 V, 700 V, 900 V, 1100 V and 1300 V gives

1.29, 1.90, 2.39, 2.78, 3.09, 3.41 sputtering yield for Ni respectively and 0.4451, 0.6364, 0.7810, 0.8876, 0.9856, 1.07 for Ti respectively. The energy of the Ni atom after ejection from the surface are 18.45 eV/atom, 20.64 eV/atom, 22.20 eV/atom, 24.01 eV/atom, 25.33 eV/atom, 26.39 eV/atom and for Ti 23.44 eV/atom, 28.66 eV/atom, 32.52 eV/atom, 36.42 eV/atom, 39.91 eV/atom, 42.67 eV/atom respectively for 300 V, 500 V, 700 V, 900 V, 1100 V and 1300 V (Figure 2(b)).

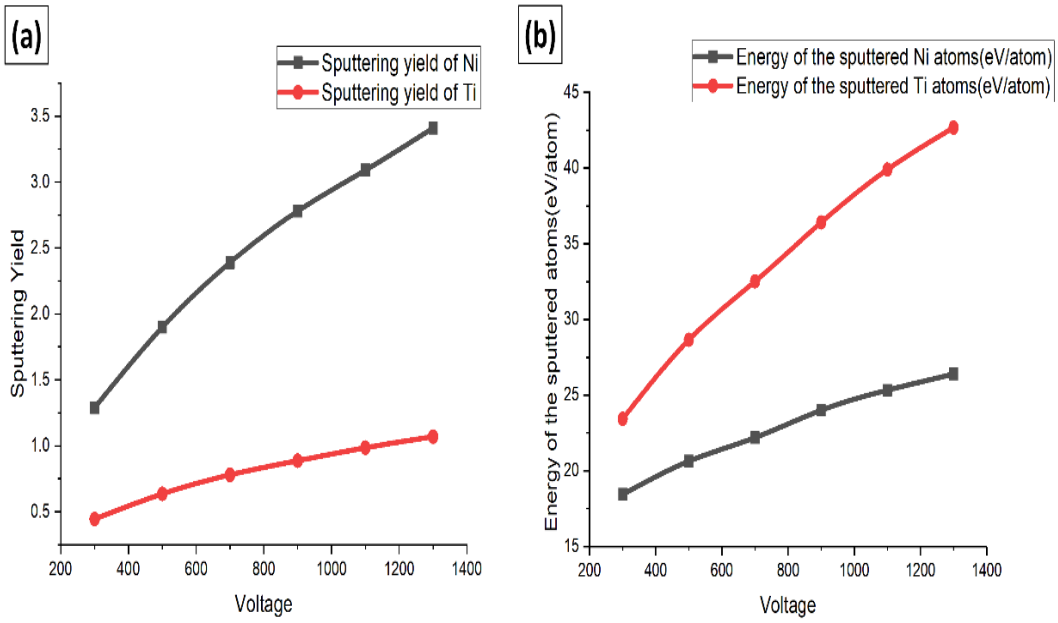

Figure 2: Sputtering yield of Ni and Ti at different voltage.

Figure 3 and figure 4 gives the target surface damage depth with respect to the voltage change for both Ni and Ti target respectively. The plot was obtained after the simulation of 90000 ions was completed to get precise results. It is observed that for Ni, the target surface atom ejected from 20 A depth at 300 V and gradually increases the depth up to 50 A at 1300 V. whereas, in case of Ti target, the surface atom ejection occurred from 30 A at 300 V and gradually increases up to 100 A at 1300 V. by comparing both the target atom ejection, it is observed that the ejection of Ti atom is in a more scattered way. The ions marked in blue in the figures above have stopped moving after losing energy in many collisions. It is seen that as the voltage is increased, the area of the damaged site is also growing. This also indicates

that the sputtering yield is increasing with increasing voltage. Sputtered atoms of Ti has more energy than that of Ni. This signifies that there will be different amount of energy transmitted to the substrate from different targets when co-sputtering is carried out. It may lead to non-uniformity of homogenization throughout the substrate surface. So batchwise sputtering with predefined thickness is essential which will be followed by the annealing process [18].

Figure 3: Target surface damage depth vs voltage at (a) 300 V (b) 500 V (c) 700 V (d) 900 V (e) 1100 V (f) 1300 V of Ni target

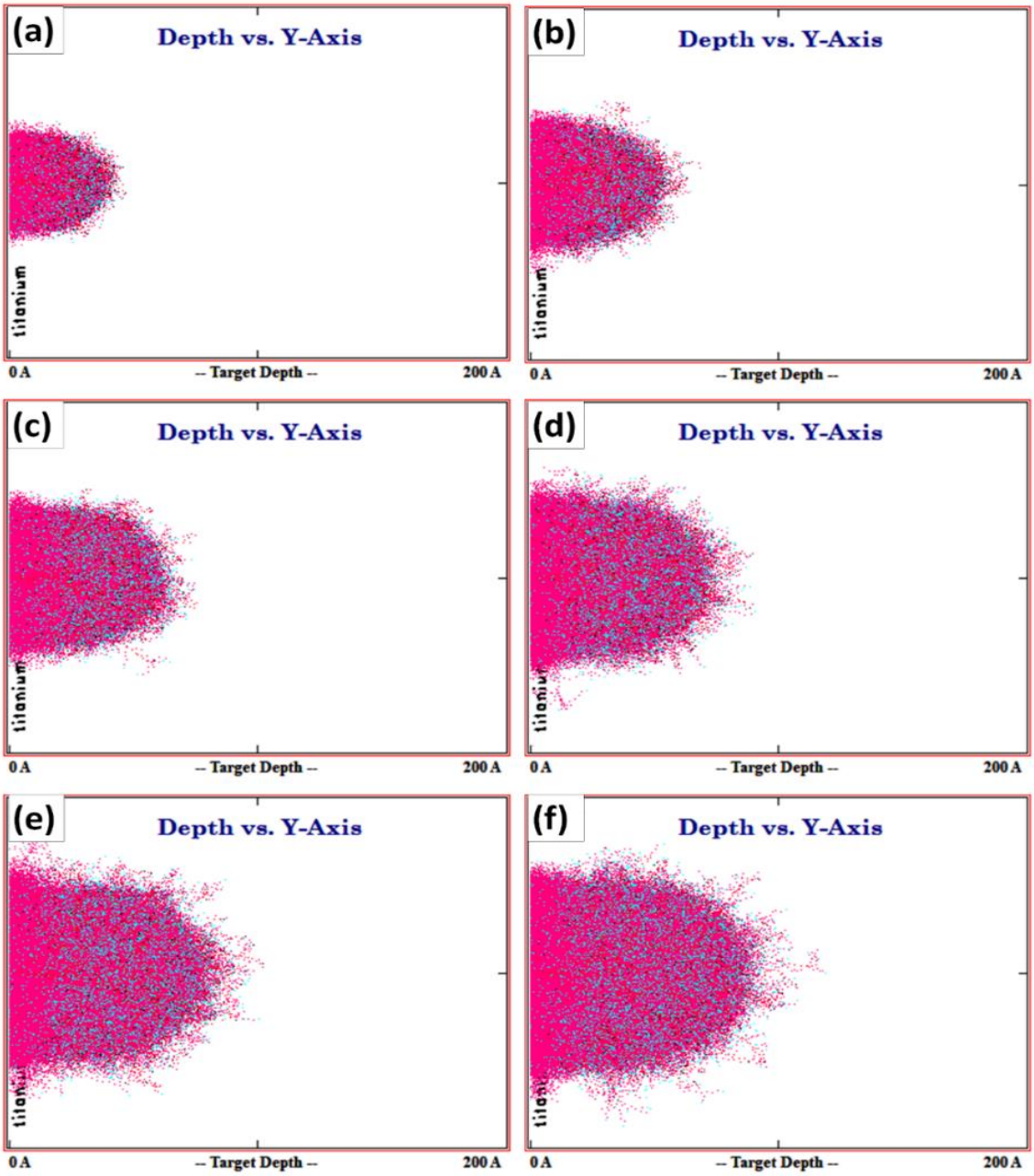

Figure 4: Target surface damage depth vs voltage at (a) 300V (b) 500V (c) 700V (d) 900V (e) 1100V (f) 1300V of Ti target

3.2. Sputtering yield with variation of the angle of incidence of ions

Deposition efficiency greatly influenced by the angle of incident of adatom to the substrate surface. Figure 5 shows the variation of sputtering yield of Ni and Ti at different angle of incidence. At 30° angle of incidence, for voltage 300 V, 500 V, 700 V, 900 V, 1100 V and 1300 V, sputtering yield of Ni 1.39 , 2.14, 2.74, 3.27, 3.69, 4.08 respectively (figure 5a), and

sputtering yield of Ti is 0.5142, 0.7630, 0.9601, 1.12, 1.26, 1.38 respectively (figure 5b). At 45° angle of incidence, for voltage 300 V, 500 V, 700 V, 900 V, 1100 V and 1300 V, sputtering yield of Ni is 1.55, 2.47, 3.23, 3.91, 4.46, 4.97 respectively, and sputtering yield of Ti is respectively. Figure 6 and figure 7 shows structural presentation of target surface damage at 30° angle of incidence with variation of voltage for nickel target and Ti target respectively. Similarly for 45° angle of incidence, for nickel target and Ti target has been shown in figure 8 and figure 9.

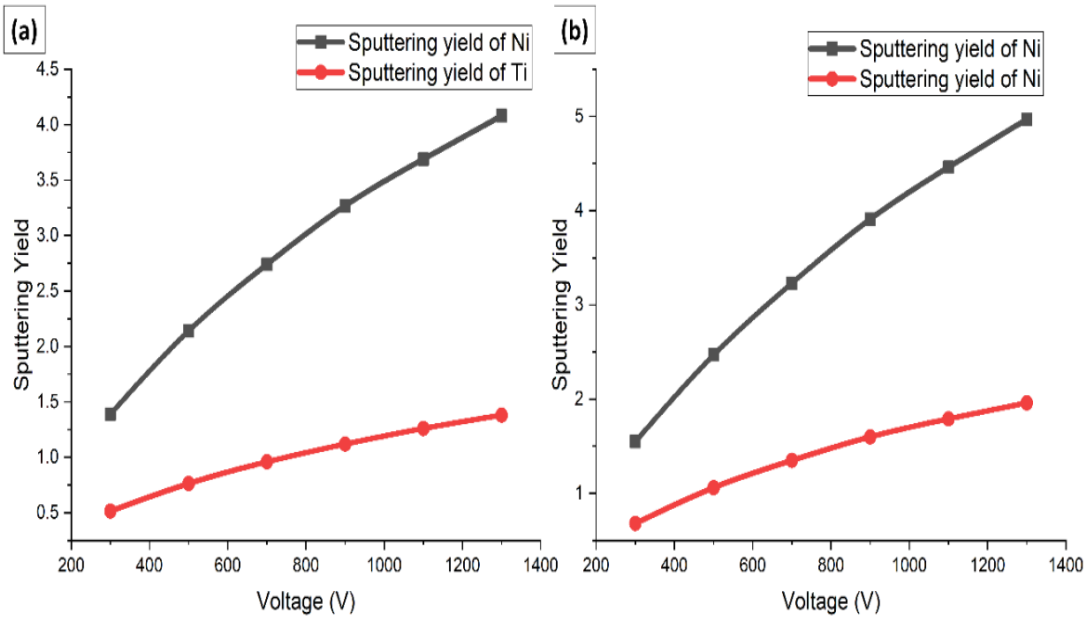

Figure 5: Sputtering yield of Ni and Ti at angle of incidence: (a) 30° and (b) 45°

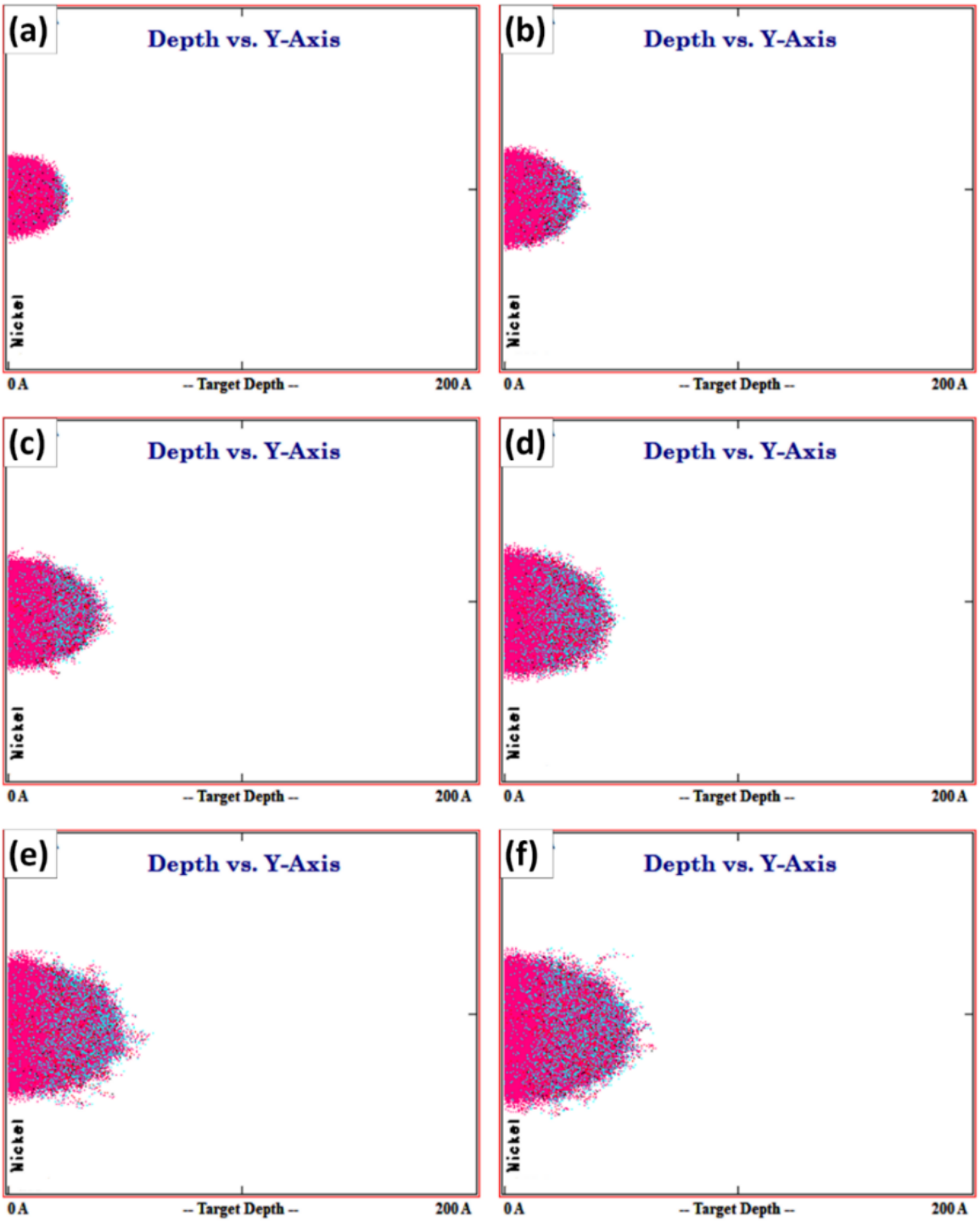

Figure 6: Target surface damage at 30° angle of incidence and at voltage of (a) 300V (b) 500V (c) 700V (d) 900V (e) 1100V (f) 1300V of nickel target.

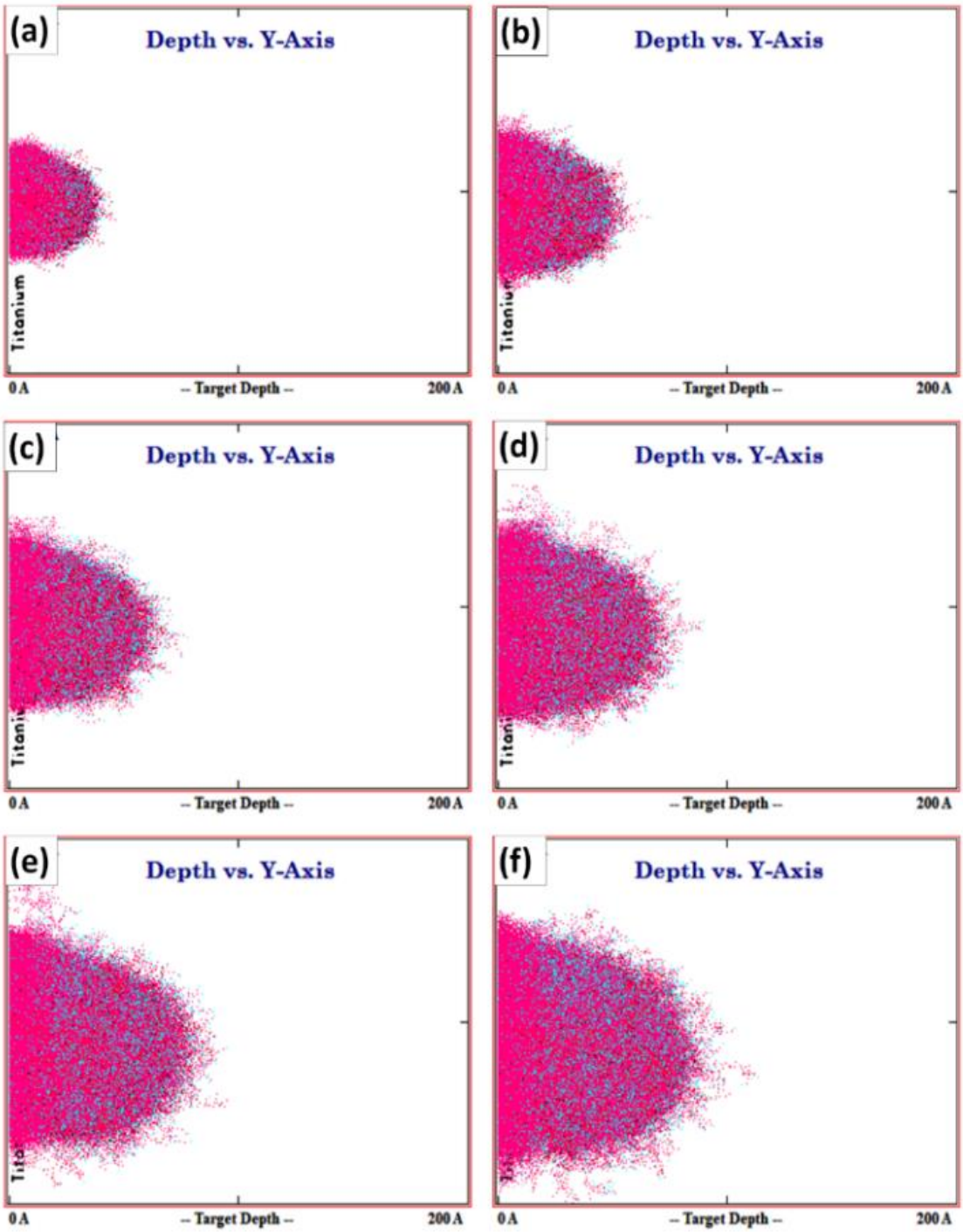

Figure 7: Target surface damage at 30° angle of incidence and at voltage of (a) 300V (b) 500V (c) 700V (d) 900V (e) 1100V (f) 1300V of titanium target.

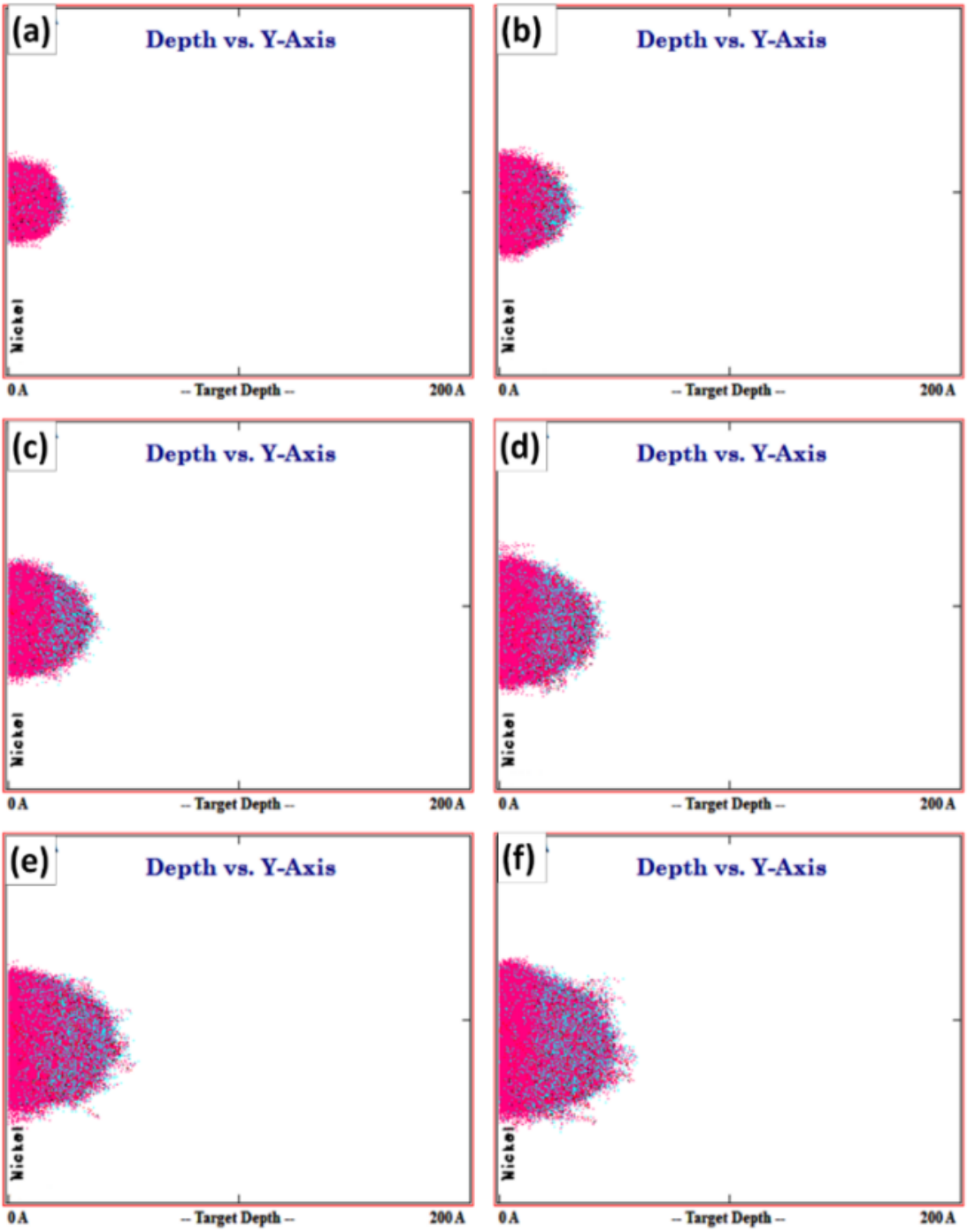

Figure 8: Target surface damage at 45° angle of incidence and at voltage of (a) 300V (b) 500V (c) 700V (d) 900V (e) 1100V (f) 1300V of nickel target.

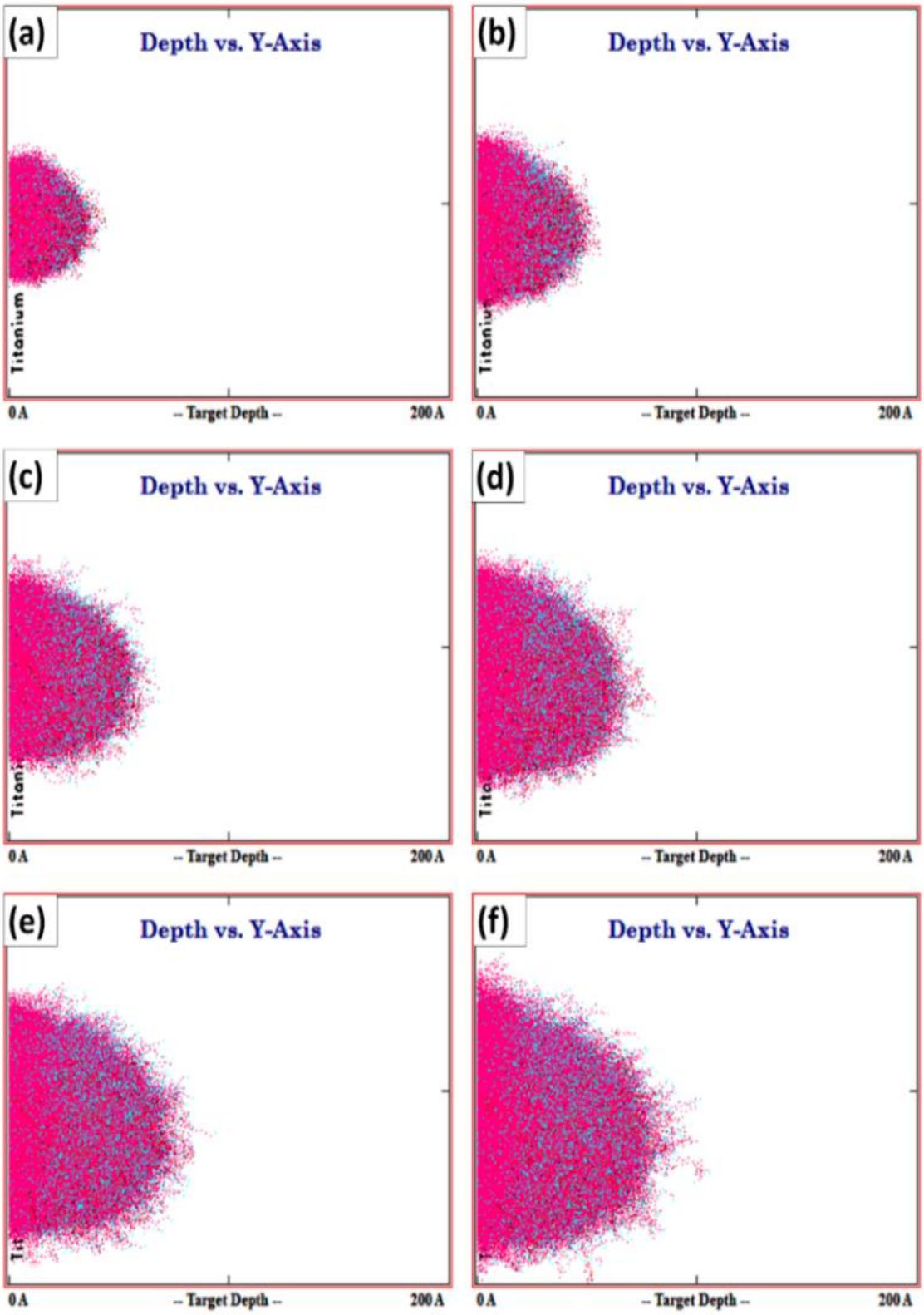

Figure 9: Target surface damage at 45° angle of incidence and at voltage of (a) 300V (b) 500V (c) 700V (d) 900V (e) 1100V (f) 1300V of titanium target.

It is found that the sputtering yield increases as the angle of incidence is increases from 30° to 45°. In addition, the sputtering yield of nickel is more than titanium at a particular angle. It can found that the sputtering yield is increasing to a maximum value at nearly 70°, and there after continues to decreases. This happens because if the incident angle is less than 70°, a significant portion of the energy is distributed near the surface. This raises the chances of a surface atom receiving sufficient energies to sputter. At higher angle sputtering yield starts decreasing after attaining the maximum value which is due to multiple reflection [19].

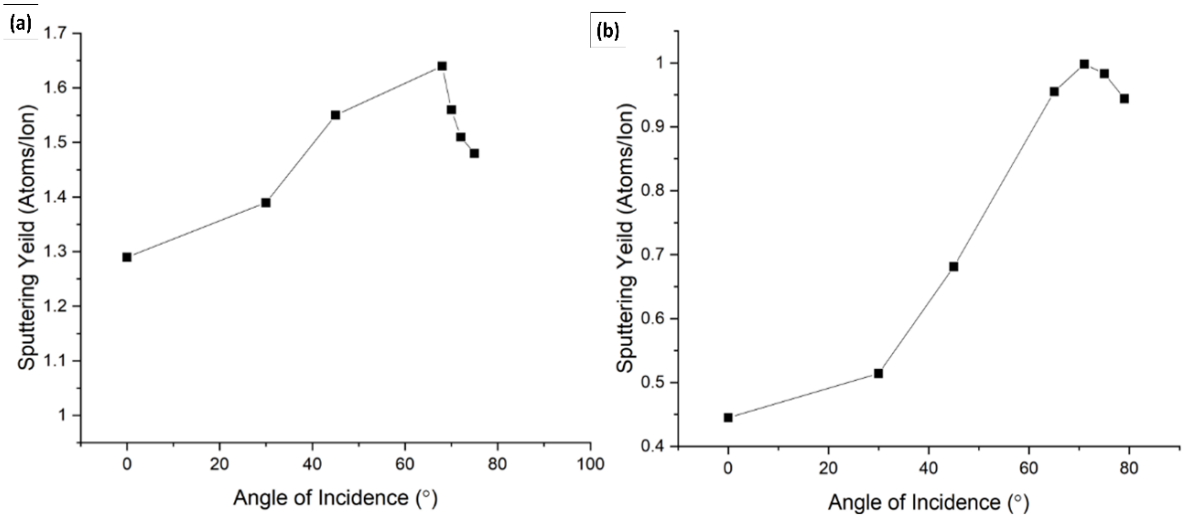

Figure 10: Variation of sputtering yield with increase in angle of incidence of (a) Ni target, and (b) Ti target.

3.3. Energies involved in sputtering with variation of the thickness

Film thickness has been varied such as 800Å, 1000Å, 1200Å at respective energies obtained from SRIM table. Table 3 shows the input parameters for simulation for various thickness.

Table 3: Input parameters for simulation

Width(Å)	Energy(keV)	Angle of incidence	Total number of ions
800	145	0°	4000
1000	190	0°	4000
1200	210	0°	4000

The number of ions increases with the 145keV energy to observe the behavior of the ions at film thickness of 800Å (figure 11). The backscattered ion and transmitted ion outputs has been obtained at different time step, as mentioned in the table 4.

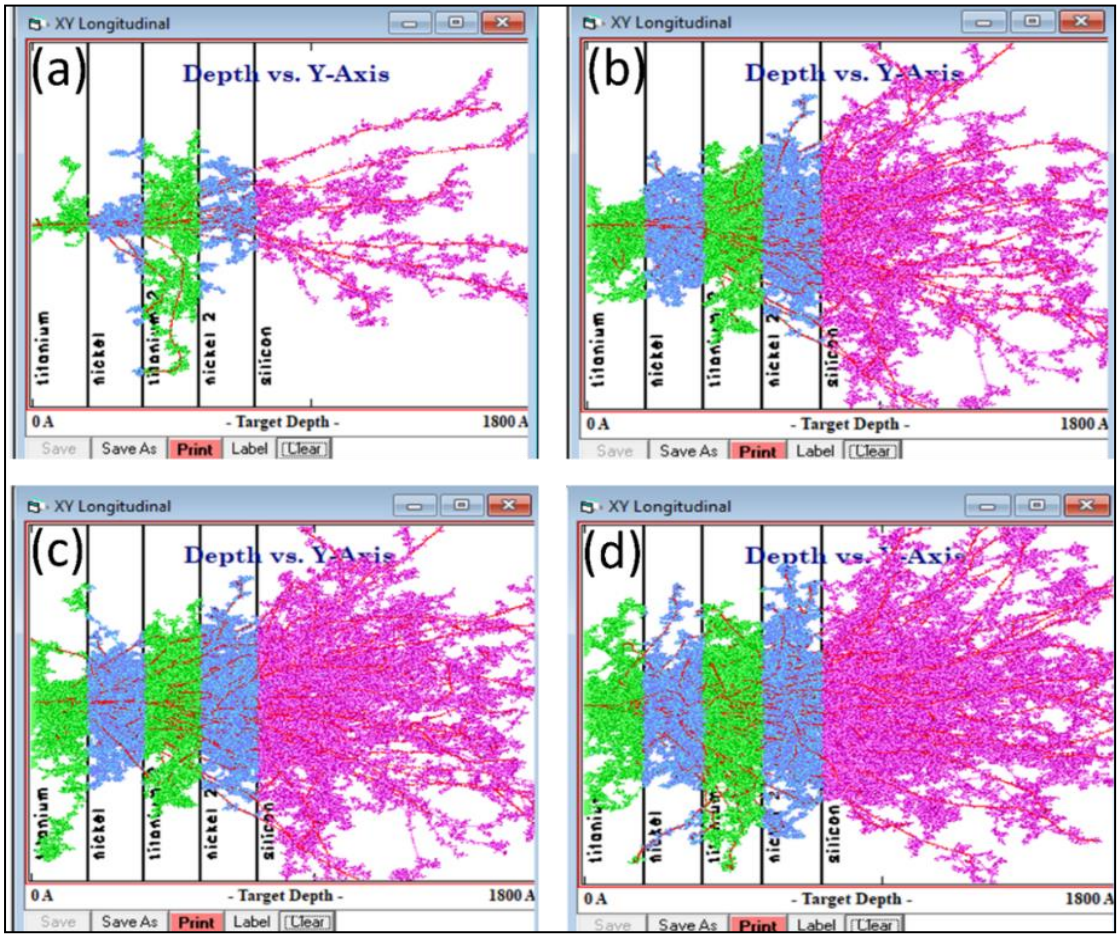

Figure 11: depth vs Y-axis at film thickness of 800Å and 145keV taken at time-step of (a) 1000 ions (b) 2000 ions (c) 3000 ions (d) 4000 ions.

Table 4: Output values after simulation showing back-scattered ion, transmitted ions and vacancies for 800Å

Time-step (no. of ions)	Back-scattered ions	Transmitted ions	Vacancies
1000	3	32	2451
2000	7	56	2453
3000	12	89	2455
4000	12	116	2456

For the film thickness of 1000 Å, the number of ions increases with the 190 keV (figure 12). The back-scattered ions, transmission ions and the number of vacancies increases with increased time step i.e. the number of ions (table 5).

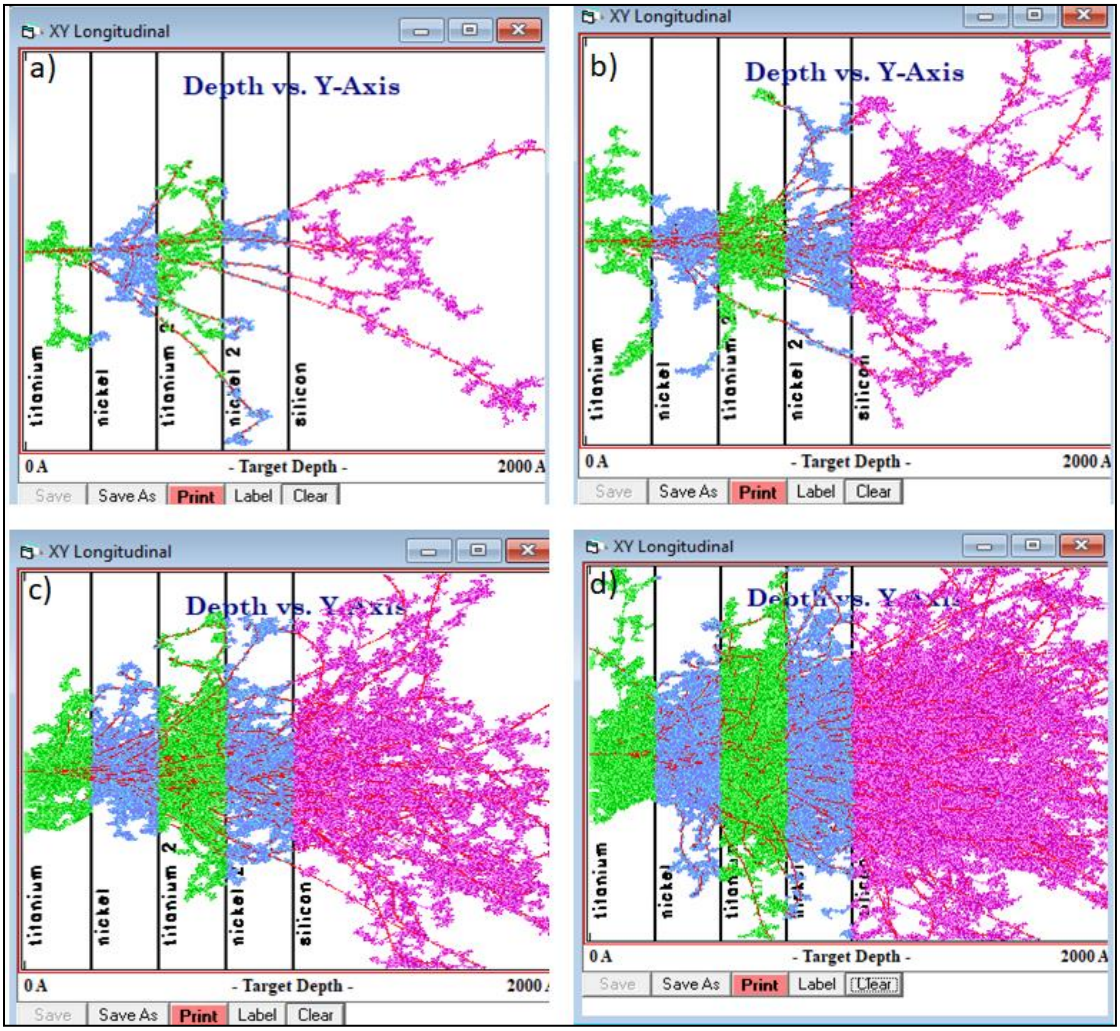

Figure 12: Depth vs Y-axis at film thickness of 1000Å and 190keV at time-step of (a) 1000 ions (b) 2000 ions (c) 3000 ions (d) 4000 ions

Table 5: Output values after simulation showing back-scattered ion, transmitted ions and vacancies for 1000Å.

Time steps (no. of ions)	Back-scattered ions	Transmitted ions	Vacancies
1000	2	84	2981
2000	4	202	2979
3000	8	292	2990
4000	12	299	2994

For the film thickness of 1000 Å, the number of ions increases with the 210 keV (figure 13). The back-scattered ions, transmission ions and the number of vacancies increases with increased time step i.e. the number of ions (table 6).

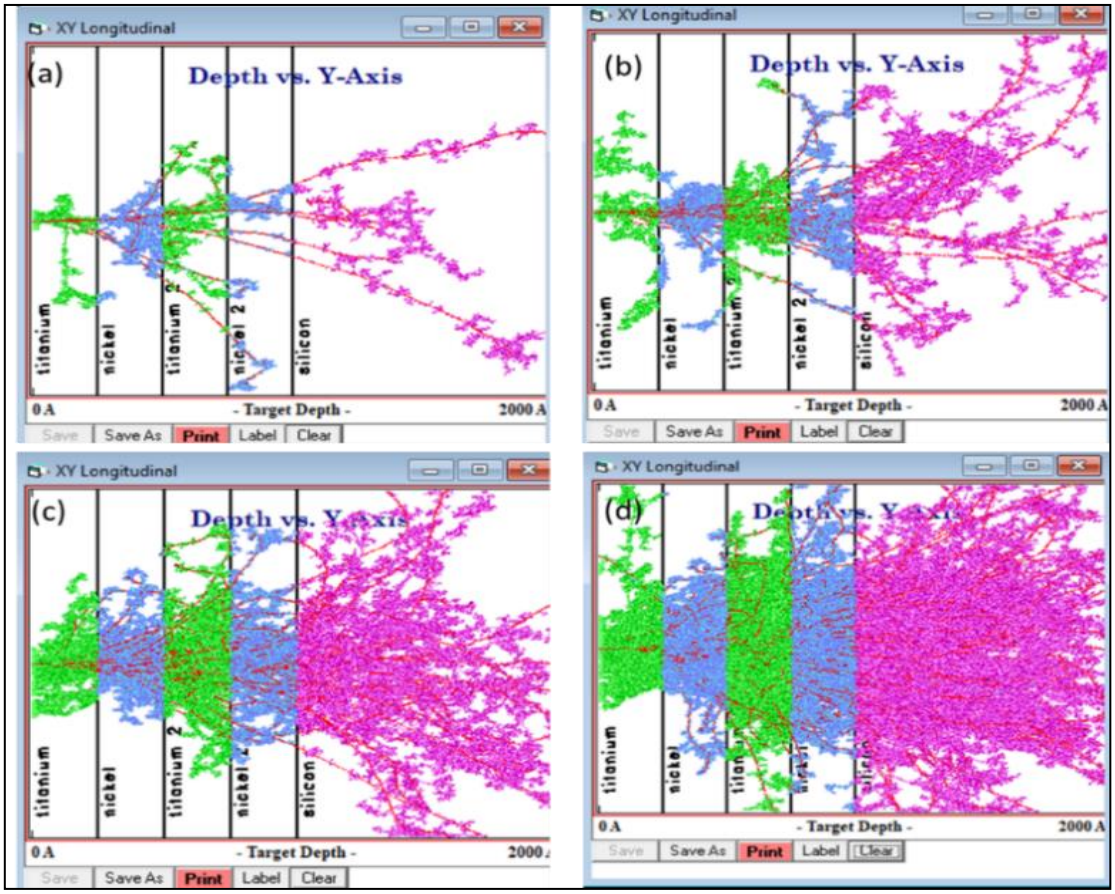

Figure 13: depth vs Y-axis at film thickness of 1200Å and 210keV at time-step of (a) 1000 ions (b) 2000 ions (c) 3000 ions (d) 4000 ions

Table 6: Output values after simulation showing back-scattered ion, transmitted ions and vacancies for 1200 Å.

Time steps (no. of ions)	Back-scattered ions	Transmitted ions	Vacancies
1000	1	66	3264
2000	3	136	3253
3000	4	150	3250
4000	5	237	3252

3.3.1. Ion range graph at different film thickness

The distribution of argon ions in the targets is seen for different thickness. It is found that the ion range increases with increase in width of the thin film (figure 14 a-c). For the thickness 800 Å, 1000 Å, 1200 Å, the ion range are 820 Å, 1027 Å, 1107 Å respectively. The skewness indicates the spread ability of the ion range. Skewness represents a bias towards preferential direction with respect to the perpendicular direction whereas kurtosis represents how heavily the tails of a distribution differ from the tails of a normal distribution. For 800 Å, 1000 Å, and 1200 Å, the skewness is 0.4209, 0.2416, and 0.2631 respectively and kurtosis is 2.4647, 2.3074, 2.5498 respectively.

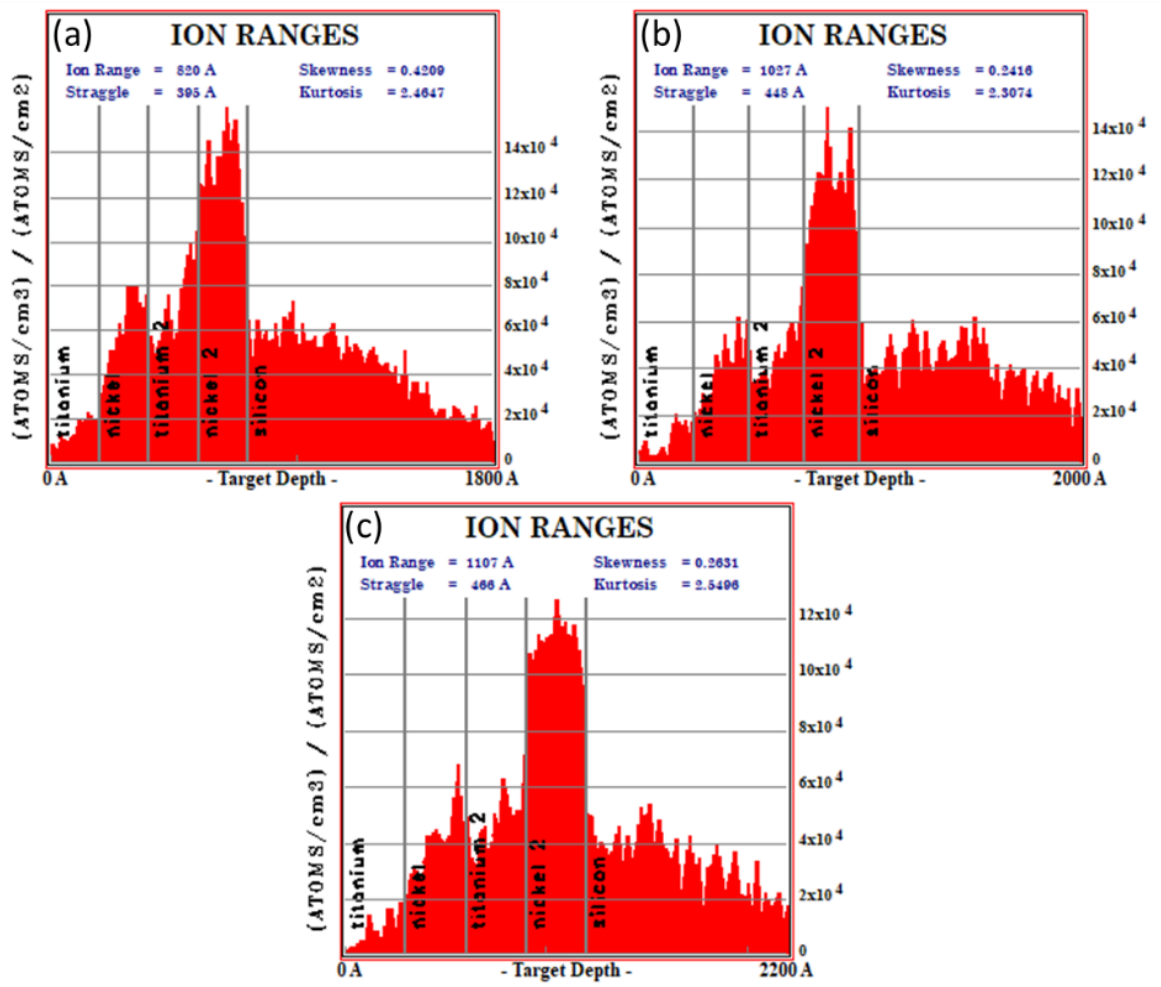

Figure 14: ion distributions at (a) 800Å (b) 1000Å (C) 1200Å

3.3.2. Atom distribution graph at different layer

Figure 15 shows the ion distribution at each of the successive layer. The silicon recoil distribution is depicted in pink, titanium in green and nickel in blue. These indicate all the atoms have been deposited on the silicon substrate. The peak of the Ti atom distribution (green) is lower than that of the Ni atoms ions. This indicates sputtering yield of Ti is less. The peaks are of different size so they contribute differently to the thin film deposition. This plot's units is "(Atoms/cm3)/ (Atoms/cm2)" [20].

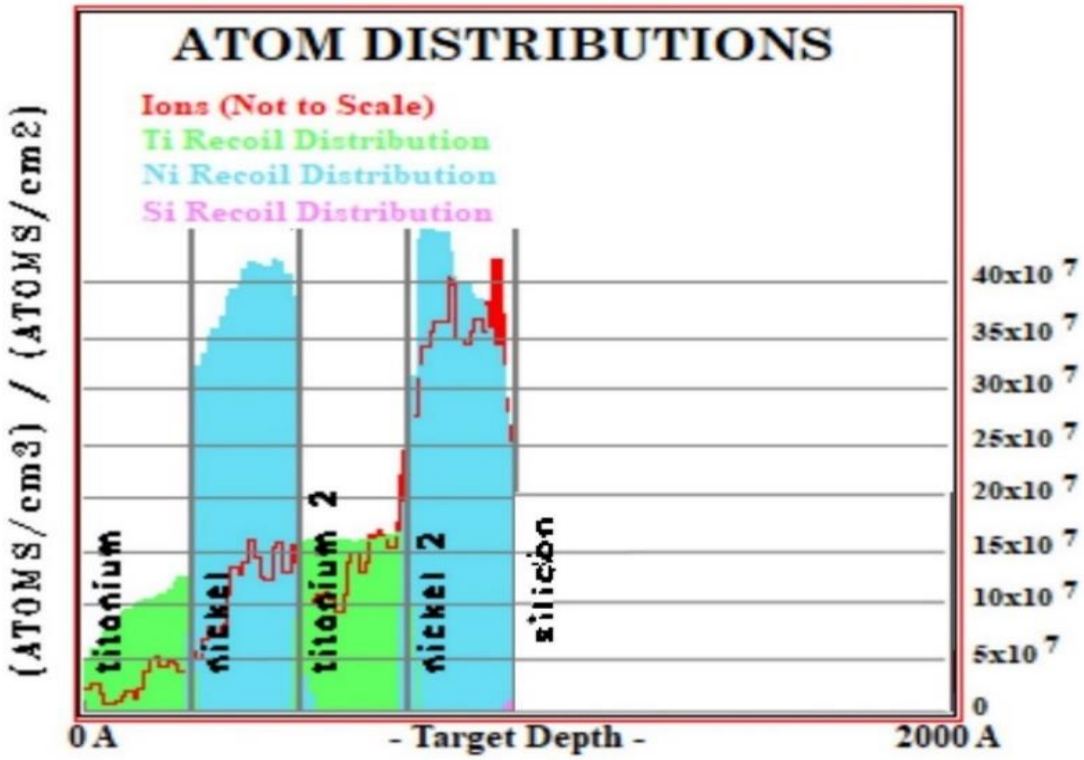

Figure 15: Atom distributions graph

3.3.3. Energy absorbed and energy loss by targets with respect to the sputtering yield

Figure 16 shows the energy required to break the binding energy of the surface atom. It depicts how target atoms will absorb. From figure we can see that energy absorbed by nickel is more that is why Ni atoms get sputtered more than titanium. It is found that for the thickness 800 Å, 1000 Å, 1200 Å, the energy absorbed by the target is 32%, 37%, and 38 %

respectively and the energy loss by the argon atoms are 68%, 63%, and 62% respectively before deposition at the substrate surface.

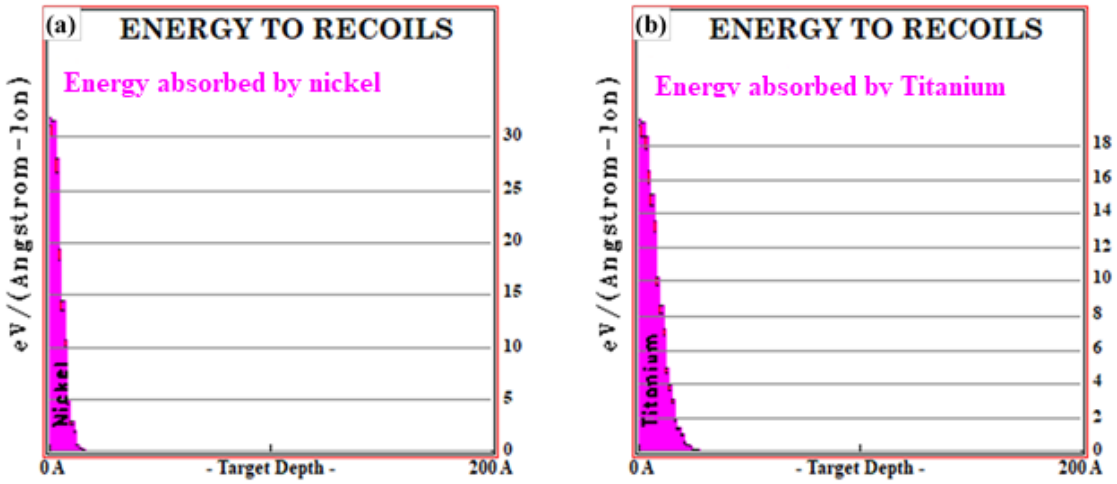

Figure 16: Energy absorbed by targets from energetic argon ions: (a) Nickel (b) Titanium

3.3.4. Sputtering yield of a single atom to estimate the use of NiTi target for the sputtering process

Figure 17 shows the integral sputtering. This graph depicts the energy of every recoiling particle that hits the surface of the targets. As the ordinate is measured in Atoms/Ion, each ion will produce around as many recoiling atoms that will reach the surface. The Esurf, for NiTi targets is estimated to be 4.7eV (depicted by vertical line in the graph). The atom which is on left of the line is not sputtered since the energy is less than 4.7 eV. The number of atoms getting sputtered is thenumber of atoms hitting the target surface with energy higher than 4.7 eV, and it correlates to the sputtering yield table in the SRIM-TRIM softwere. The integral plot shows how many atoms with energies greater than a specific threshold reach the surface. The differential sputtering graph shows the distribution of atom energies hitting the surface. Therefore we have increase the energy level of primary gas atom to reach the energy level 4.7 ev for each of the atom for better deposition efficiency for NiTi [21-22].

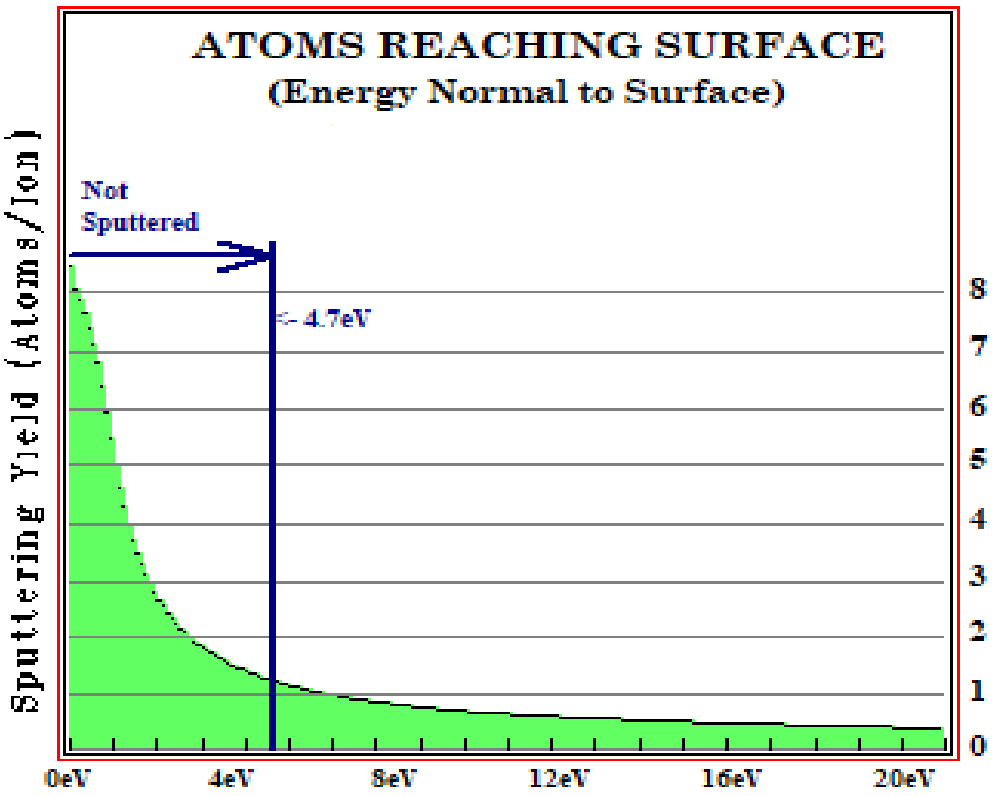

Figure 17: Sputtering graph

3.4. Surface and interface morphology using optimized parameters

As per the optimized thickness with respect to the energy requirement, 1000 A (100 nm) thickness has been developed on the Si substrate. Figure 18(a) shows the surface morphology of double bi-layered NiTi thin films. This figure shows compact depositions looks like an orange peel type of island without any surface cracks. Due to treatment at high temperature, atomic migration plays a great role for the surface smoothness [23]. Still a little amount of pores is detected in between the consecutive orange peel type island. As comparison with the as-deposited sample, 600 annealed samples has low porosity, less surface roughness, less inter granular crack and little higher oxidation on the surface. Figure 18 shows the interfacial morphology of a double bi-layered NiTi thin film. In Figure 18 (b) diffusion in between layers has occurred. For better diffusion among developed layer, annealing can be done around 500 ºC to get a homogenized structure essential for shape memory behavior [14, 24].

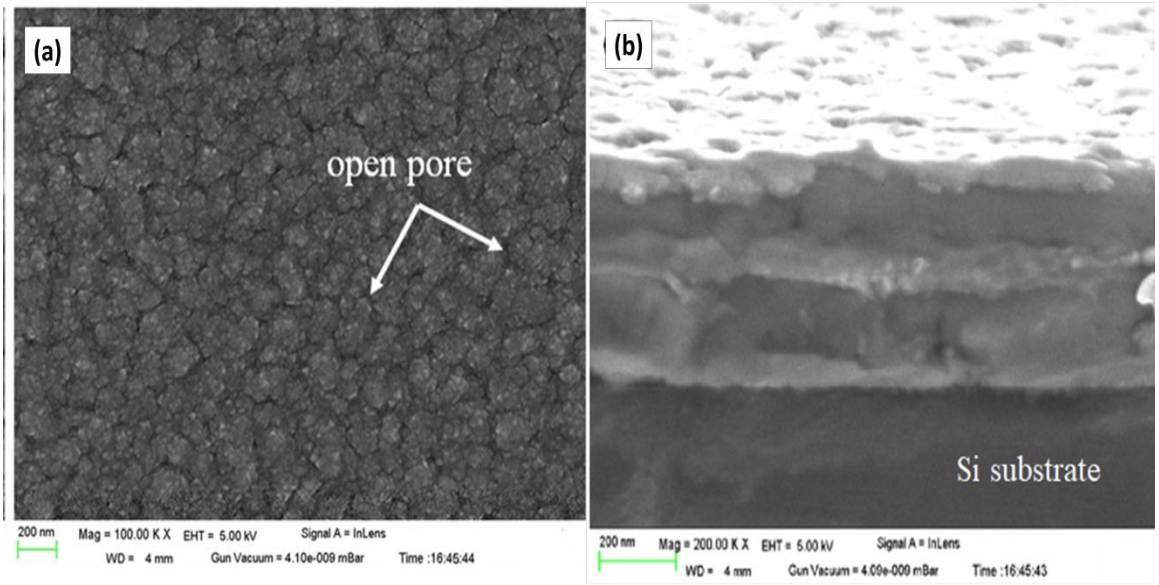

Figure 18: FESEM micrograph of (a) surface, and (b) interface of double bi-layered NiTi thin films

4. Conclusions

The following results were found after completing numerous simulations on the SRIM and TRIM software and tests on a sputtering deposited double bi-layered NiTi thin film:

- With increase in energy input i.e. target voltage, the sputtering yield also increases. Sputtering yield of Ni is more than Ti indicating that Ni can be removed relatively easier than Ti, and this indicates average surface binding energy of Ni is less than Ti. If the impact energy is less than average surface binding energy then sputtering does not occur.
- With increasing voltage, the amount of energy delivered by the atoms to the surface rose significantly, indicating that more energetic particles are indeed being deposited. Energy absorbed by nickel atoms is more than titanium atoms which explains why sputtering yield of Ni is more than Ti.
- With increasing angle of incidence the sputtering yield increases for Ni and Ti as well, but Ni have more sputtering yield than Ti. With increase in angle of incidence

sputtering yield reaches maximum up to 77° and thereafter it starts decreasing due to increase in reflection.

- As the time-step (number of ions) in the simulations increases the damage of the target is visible clearly. As the time-step increases the back-scattered ions, transmitted ions and no. of vacancies of the target increases.
- As the thickness of the film (width) increases, the number of back-scattered ions decreases. This is because the thickness of film is increased and therefore the ions cannot return back as it has to travel a longer distance and it loses its energy gradually.

The results of the current study and their analyses relate to the subsequent directions for future research, which directs research in several NiTi thin film SMA domains. The current study has increased the possibility of recognizing the handling of double bi-layer Ni-Ti thin films for MEMS devices. The current simulation using SRIM and TRIM software has increased the possibilities for understanding sputtering of Ni/Ti targets. Through the modeling tool, efforts are undertaken to comprehensively examine the influence of numerous parameters on the sputtering process. To find out the diffusion at a relatively long time-step, modelling with Monti-carlo simulation can be used.

Acknowledgement

There exist no financial conflicts in this work.

References

1. J. V. Humbeeck, Non-medical applications of shape memory alloys, Materials Science and Engineering: A, Volumes 273–275, 1999, Pages 134-148, ISSN 0921-5093, https://doi.org/10.1016/S0921-5093(99)00293-2.
2. J. Mohd Jani, Martin Leary, Aleksandar Subic, Mark A. Gibson, A review of shape memory alloy research, applications and opportunities, Materials & Design (1980-

2015), Volume 56, 2014, Pages 1078-1113, https://doi.org/10.1016/j.matdes.2013.11.084.

3. Z. Song, Hui-Hui Dai, Qing-Ping Sun, Propagation stresses in phase transitions of an SMA wire: New analytical formulas based on an internal-variable model, International Journal of Plasticity, Volume 42, 2013, Pages 101-119, https://doi.org/10.1016/j.ijplas.2012.10.002.
4. A. Behera, (2022). Shape-Memory Materials. In: Advanced Materials. Springer, Cham. https://doi.org/10.1007/978-3-030-80359-9_1
5. Ajit Behera, P. Parida and A. Kumar, “Chapter Title: NiTi thin film shape memory alloy and their industrial application, Book title: “Functional Materials and Advanced Manufacturing” CRC Press, 2020, DOI: 10.1201/9780429298042-9. https://www.taylorfrancis.com/books/e/9780429298042/chapters/10.1201/9780429298042-9.
6. B. C. G. Marupalli, Ajit Behera, S. Aich, A critical review on Nickel-Titanium thin film shape memory alloy fabricated by Magnetron Sputtering and influence of process parameters, Transactions of the Indian Institute of Metals, https://doi.org/10.1007/s12666-021-02418-z.
7. [A. Behera, Dipen Kumar Rajak, Reza Kolahchi, Maria-Luminiţa Scutaru, Catalin I. Pruncu, Current global scenario of Sputter deposited NiTi smart systems, Journal of Materials Research and Technology, Vol. 9, Issue 6, 2020, 14582-14598, https://doi.org/10.1016/j.jmrt.2020.10.032.
8. S. Kumar Patel, A. Behera, Evolution of Phases and their Influence on Shape Memory Effect by Varying Sintering Parameters of NiTi Alloys, Metals and Materials International, 2022, DOI: 10.1007/s12540-021-01166-5.
9. H Kahn1, M A Huff2 and A H Heuer, The TiNi shape-memory alloy and its applications for MEMS, J. Micromech. Microeng. 8 213, https://doi.org/10.1088/0960-1317/8/3/007
10. A. David Johnson, Valery Martynov, and Vikas Gupta "Applications of shape memory alloys: advantages, disadvantages, and limitations", Proc. SPIE 4557, Micromachining and Microfabrication Process Technology VII, (28 September 2001); https://doi.org/10.1117/12.442964
11. B. S. Shariat, Qinglin Meng, Abdus S. Mahmud, Zhigang Wu, Reza Bakhtiari, Junsong Zhang, Fakhrodin Motazedian, Hong Yang, Gerard Rio, Tae-hyun Nam, Yinong Liu, Functionally graded shape memory alloys: Design, fabrication and experimental

evaluation, Materials & Design, Volume 124, 2017, Pages 225-237, https://doi.org/10.1016/j.matdes.2017.03.069.

12. A. Biesiekierski, James Wang, Mohamed Abdel-Hady Gepreel, Cuie Wen, A new look at biomedical Ti-based shape memory alloys, Acta Biomaterialia, Volume 8, Issue 5, 2012, Pages 1661-1669, ISSN 1742-7061, https://doi.org/10.1016/j.actbio.2012.01.018.
13. T Mineta, Y.Haga, (2011). Materials and Processes in Shape Memory Alloy. In: Ghodssi, R., Lin, P. (eds) MEMS Materials and Processes Handbook. MEMS Reference Shelf, vol 1. Springer, Boston, MA. https://doi.org/10.1007/978-0-387-47318-5_6
14. A. Behera, S. Aich, "Characterization and properties of magnetron sputtered nanoscale NiTi thin film and the effect of annealing temperature", Surf. Interface Anal. 47, 2015, 805-814, https://doi.org/10.1002/sia.5777.
15. J. F. Ziegler, Biersack, J.P. (1985). The Stopping and Range of Ions in Matter. In: Bromley, D.A. (eds) Treatise on Heavy-Ion Science. Springer, Boston, MA. https://doi.org/10.1007/978-1-4615-8103-1_3
16. J. W. Wilson, F.A. Cucinotta, H. Tai, J.L. Shinn, S.Y. Chun, R.K. Tripathi, L. Sihver, Transport of light ions in matter, Advances in Space Research, Volume 21, Issue 12, 1998, pages 1763-1771, https://doi.org/10.1016/S0273-1177(98)00063-5.
17. Y. Okajima, Estimation of sputtering rate by bombardment with argon gas ions, Journal of Applied Physics 51, 715 (1980); https://doi.org/10.1063/1.327331
18. A. Behera, R. Suman, S. Aich, S.S. Mohapatra, Sputter-deposited Ni/Ti double-bilayer thin film and the effect of intermetallics during annealing, Surface Interface Anal., 2016, Volume 49, Issue 7, July 2017, Pages 620–629 DOI: 10.1002/sia.6201.
19. J. P. Biersack, W. Eckstein, Sputtering studies with the Monte Carlo Program TRIM.SP. Appl. Phys. A 34, 73–94 (1984). https://doi.org/10.1007/BF00614759
20. Peter Sigmund, Theory of Sputtering. I. Sputtering Yield of Amorphous and Polycrystalline Targets, Phys. Rev. Volum E 184, No. 2, 184, 383 – Published 10 August 1969.
21. K. K Ho, K.P Mohanchandra, Gregory P Carman, Examination of the sputtering profile of NiTi under target heating conditions, Thin Solid Films, Volume 413, Issues 1–2, 2002, Pages 1-7, https://doi.org/10.1016/S0040-6090(02)00339-5.
22. K. K. Ho, Gregory P. Carman, Sputter deposition of NiTi thin film shape memory alloy using a heated target, Thin Solid Films, Volume 370, Issues 1–2, 2000, Pages 18-29, https://doi.org/10.1016/S0040-6090(00)00947-0.

23. A. Kumar, Devendra Singh, Davinder Kaur, Grain size effect on structural, electrical and mechanical properties of NiTi thin film deposited by magnetron co-sputtering, Surface and Coatings Technology, Volume 203, Issue 12, 2009, pages 1596-1603, https://doi.org/10.1016/j.surfcoat.2008.12.005.
24. T. Lehnert, H Grimmer, P Böni, M Horisberger, R Gotthardt, Characterization of shape-memory alloy thin films made up from sputter-deposited Ni/Ti multilayers, Acta Materialia, Volume 48, Issue 16, 2000, Pages 4065-4071,, https://doi.org/10.1016/S1359-6454(00)00189-0.